Dalton Transactions

Cite this: *Dalton Trans.*, 2011, **40**, 9752

www.rsc.org/dalton

PAPER

Role of Local and Electronic Structural Changes with Partially Anion substitution Lithium Manganese Spinel Oxides on Their Electrochemical Properties: X-ray Absorption Spectroscopy Study†

Toyoki Okumura,[a] Tomokazu Fukutsuka,[b] Keisuke Matsumoto,[a] Yuki Orikasa,[c] Hajime Arai,*[c] Zempachi Ogumi[c] and Yoshiharu Uchimoto[a]

Received 31st March 2011, Accepted 20th July 2011
DOI: 10.1039/c1dt10612k

The electronic and local structures of partially anion-substituted lithium manganese spinel oxides as positive electrodes for lithium-ion batteries were investigated using X-ray absorption spectroscopy (XAS). $LiMn_{1.8}Li_{0.1}Ni_{0.1}O_{4-\eta}F_{\eta}$ ($\eta = 0$, 0.018, 0.036, 0.055, 0.073, 0.110, 0.180) were synthesized by the reaction between $LiMn_{1.8}Li_{0.1}Ni_{0.1}O_4$ and NH_4HF_2. The shift of the absorption edge energy in the XANES spectra represented the valence change of Mn ion with the substitution of the low valent cation as Li^+, Ni^{2+}, or F^- anion. The local structural change at each compound with the amount of a Jahn–Teller Mn^{3+} ion could be observed by EXAFS spectra. The discharge capacity of the tested electrode was in the order of $LiMn_2O_4 > LiMn_{1.8}Li_{0.1}Ni_{0.1}O_{4-\eta}F_{\eta}$ ($\eta = 0.036$) > $LiMn_{1.8}Li_{0.1}Ni_{0.1}O_4$ while the cycleability was in the order of $LiMn_{1.8}Li_{0.1}Ni_{0.1}O_{4-\eta}F_{\eta}$ ($\eta = 0.036$) ≈ $LiMn_{1.8}Li_{0.1}Ni_{0.1}O_4 > LiMn_2O_4$. It was clarified that $LiMn_{1.8}Li_{0.1}Ni_{0.1}O_{4-\eta}F_{\eta}$ has a good cycleability because of the anion doping effect and simultaneously shows acceptable rechargeable capacity because of the large amount of the Jahn–Teller Mn^{3+} ions in the pristine material.

1. Introduction

Lithium-ion batteries (LIB) with high energy density, safety, and durability are required for electric vehicles (EV), hybrid electric vehicles (HEV), and plug-in hybrid electric vehicles (PHEV) as their power sources. Lithium manganese spinel oxide $LiMn_2O_4$ is one of the candidates for the positive electrode materials for LIBs as an alternative to the conventional $LiCoO_2$ cathode because of its low cost and low toxicity.[1,2] However, the capacity fading during the charge-discharge cycle is one of the serious problems. It is thought that this phenomenon is caused by the disproportional reaction of Mn^{3+} accompanied with dissolution of Mn^{2+} into the electrolyte, unstable surface structure of $LiMn_2O_4$ at charged states, or local structural distortion of MnO_6 octahedra by the Jahn–Tellar effect.[3,4] Several research groups have investigated the electrochemical properties of partially cation-doped lithium manganese spinel oxides $LiMn_{2-y}M_yO_4$ (M = Li, Al or the other transition metals such as Cr and Ni)[5–13] and shown that the cycleability is improved with the cation doping. The average structure, the local structure, and the electronic structure and their relationships with electrochemical properties have been investigated for these cation-doped lithium manganese spinel oxides by using X-ray diffraction measurement (XRD) and X-ray absorption spectroscopy (XAS) technique. However, this cation doping increases the average oxidation state of Mn from 3+ to 4+, leading to the decrease of the reversible capacity. In other word, the increase of Mn^{3+} in the pristine material is directly linked with the increase of the reversible capacity. Hence, it is desirable to decrease the average oxidation state of Mn (increase the amount of Mn^{3+}) while remaining good cycleability owing to the cation doping effect.

Anion-substitution has not been well studied for the lithium manganese spinel oxides compared with the cation-substitution. The radius of F^- is close to that of O^{2-}, and the electronegativity of fluorine is the largest of all elements. Hence, the substitution of O^{2-} by F^- can occur and would change the structure and electrochemical properties of lithium manganese spinel oxides. If O^{2-} is substituted by F^-, the average oxide state of Mn can be decreased and reversible capacity can be increased. In regard to cathode materials such as $LiNiO_2$ and $LiCoO_2$ for LIBs, there are some reports about the substitution of O^{2-} by F^-.[14,15] It has been reported that LiF is added to the starting materials as a fluorine source and the resulting $LiNiO_2$ and $LiCoO_2$ show better cycleability. For lithium manganese spinel oxides, there are also some reports about F^--substitution. A

[a]*Department of Interdisciplinary Environment, Graduate School of Human and Environmental Studies, Kyoto University, Yoshida-nihonmatsu-cho, Sakyo-ku, Kyoto, 606-8501, Japan*
[b]*Department of Interdisciplinary Environment, Graduate School of Engineering, Kyoto University, Nishikyo-ku, Kyoto, 615-8510, Japan*
[c]*Society-Academia Collaboration for Innovation, Kyoto University, Nishikyo-ku, Kyoto, 615-8510, Japan. E-mail: h-arai@saci.kyoto-u.ac.jp*
† Electronic supplementary information (ESI) available: See DOI: 10.1039/c1dt10612k

F^--substitution method by surface fluorination of $LiMn_2O_4$ has been carried out by Yonezawa *et al.*[16] In their report, $LiMn_2O_4$ has been treated with F_2 gas at various temperatures and it has been confirmed by X-ray photoelectron spectroscopy that the surface of $LiMn_2O_4$ has been fluorinated. Under the optimal fluorination condition, both discharge capacity and cycleability of the surface fluorinated $LiMn_2O_4$ has been better than the pristine $LiMn_2O_4$. The F^--substitution in the bulk $LiMn_2O_4$ have been carried out by Amatucci *et al.*[17] They have synthesized $Li_{1+x}Mn_{2-x}O_{4-\delta}F_z$ and $Li_{1+x}Al_yMn_{2-x-y}O_{4-\delta}F_z$ by adding LiF to the starting materials and firing at a high temperature (800 °C). The resulting spinel oxyfluoride exhibits higher discharge capacity and better cycleability than $LiMn_2O_4$. However, it has been reported that the amount of fluorine in spinel oxyfluoride is influenced by the firing temperature and the amount of fluorine is limited at high firing temperatures at which LiF can react.[18] Hence, lowering the firing temperature should be important to increase the fluorine content. Recently, Choi *et al.* reported the synthesis of spinel oxyfluoride such as $LiMn_{1.8}Li_{0.1}Ni_{0.1}O_{3.927}F_{0.073}$ at a low temperature (450 °C) by using spinel compounds and NH_4HF_2 as the starting materials.[19,20] In their reports, resulting spinel oxyfluoride shows superior electrochemical performance compared to $LiMn_2O_4$. These various reports are quite interesting, since anion substitution shows the possibility to enhance the performance of the spinel lithium manganese oxides. In order to get the guide to improve the superior electrochemical properties, understanding the detailed local/electronic structures of spinel oxyfluoride is essential. In contrast to the cation-doped compounds, such detailed structures have not been clarified for anion-substituted lithium manganese spinel oxides.

In the present paper, the local and electronic structures of the partially F^--substituted cation-doped lithium manganese spinel oxides have been respectively investigated by X-ray absorption near-edge structure (XANES) and extended X-ray absorption fine structure (EXAFS) techniques to clarify the relationship between the detailed structures and the discharge capacity profiles.

2. Experimental procedure

$LiMn_{2-x}Li_xO_4$ (x = 0, 0.05, 0.10, 0.15) and $LiMn_{1.9-y}Li_{0.1}Ni_yO_4$ (y = 0, 0.05, 0.10, 0.15, 0.20) were synthesized by the solid-state reactions. Li_2CO_3 (99.99% Kojundo Chemical Lab Industries), NiO (99.9% Furuuchi Chemical Industries), and Mn_2O_3 obtained by pre-heating of $MnCO_3$ (99.99% Kojundo Chemical Lab Industries) at 600 °C for 48 h were used as starting materials. Required amounts of starting materials were mixed and heated at 800 °C for 2 days in air, and then cooled with a rate of 0.5 °C/min. For partial fluorine substitution, the obtained $LiMn_{1.9}Li_{0.1}Ni_{0.1}O_4$ and NH_4HF_2 were mixed, and then fired at 450 °C for 5 h in air.[20] Powder X-ray diffraction measurement (RINT-2200V) with Cu-Kα radiation equipped with a graphite monochromator was used to examine the crystal structure of resulting materials. All the XRD analysis operated in the Bragg-Brentano geometry mode. XANES and EXAFS measurements were performed to investigate electronic and local structures of resulting materials on BL-7C[21] and BL-11A[22] at Photon Factory, High Energy Accelerator Research Organization Tsukuba, Japan.

For Mn and Ni K-edge, the appropriate amount of each sample for XANES and EXAFS measurements was mixed with boron nitride (BN) to obtain optimum absorption jump ($\Delta\mu t = 1$), and the mixture was pressed into pellets for the measurement. The spectra were recorded by the transmission mode using Si(111) double monochromators and a Rh-coated mirror for harmonic rejection except that they were recorded in a high-vacuum chamber by the total-electron-yield mode using a microchannel plate detector for Mn L-, O K- and F K-edges. Fourier transformations were performed using k^3 weighting. The structural parameters were determined by curve-fitting procedures using Rigaku REX2000 data analysis software.[23] The effective backscattering amplitude F_{eff}, phase correction $\gamma(k)$, and total central atom phase shift ξ were calculated with the multiple-scattering theoretical calculation program, FEFF8.20.[24] The model of $LiMn_2O_4$ was selected to input the starting parameters for the theoretical calculation. The $\chi(k)$ function was fitted according to the equation:

$$\chi(k) = \sum_i \frac{NS_0^2 |f(k,\pi)| \exp(-2\sigma_i^2 k^2) \exp(-2R_i/\lambda_i) \sin[2kR_i + \phi_i(k)]}{kR_i^2} \quad (1)$$

where N is the number of neighboring atoms, S_0^2 is the amplitude of $\chi(k)$, R is the atomic distance to the neighboring atom, σ^2 is the Debye–Waller (DW) factor, λ is the mean free path, and ϕ is the total phase shift.

Charge-discharge measurements (1/24 C) were carried out between 3.5 and 4.3 V *vs.* Li/Li^+ at room temperature using a three-electrode cell. Li foil was used as the counter and the reference electrodes, and 1 mol dm^{-3} $LiClO_4$/propylene carbonate (PC) was used as an electrolyte solution. A working electrode was a mixture of 75 wt% active material, 20 wt% acetylene black, and 5 wt% polyvinylidene difluoride (PVdF) coated onto an aluminum current collector.

Delithiated powders for Ex-situ XANES and EXAFS measurements were prepared by electrochemical method by using the three-electrode cell mentioned above, except that the mixture of 70 wt% active material, 20 wt% acetylene black, and 10 wt% poly(tetrafluoroethylene) (PTFE), pressed into paste and wrapped with Ni mesh, was used as the working electrode. Electrochemical extraction of lithium ion was carried out with constant current discharge (1/12 C). Ni mesh was removed from the paste for preparing the delithated sample. For Mn and Ni K-edge, the appropriate amount of each sample was mixed with BN to obtain optimum absorption jump ($\Delta\mu t = 1$), and the mixture was pressed into pellets for the measurements.

3. Results and Discussion

3.1. Phase identification

The XRD patterns of $LiMn_{2-x}Li_xO_4$ (x = 0, 0.05, 0.10, 0.15) and $LiMn_{1.9-y}Li_{0.1}Ni_yO_4$ (y = 0, 0.05, 0.10, 0.15, 0.20) are shown in Fig. 1. All peaks belonged to the spinel structure (*Fd-3m*) and there were no peak of impurity. The lattice parameter was calculated from the peak top method. Fig. 2 showed the plots of the lattice parameter against the content of the low valent cation (Li^+ or Ni^{2+}). In this figure, the lattice parameter was decreased monotonically with increase of low valent cation content. Taking the order of the ionic radius of $Li^+ > Ni^{2+} > Mn^{3+}$ (according to Shannon's ionic radii[25]) into account, it might happen that the lattice parameter was increased with the increment of the low

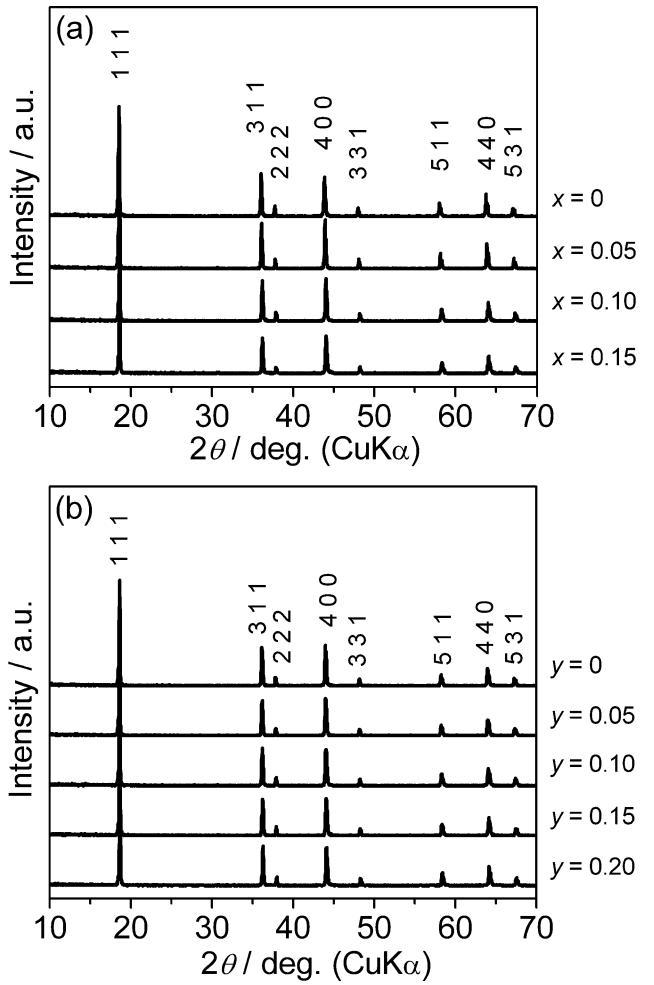

Fig. 1 Powder XRD patterns of $LiMn_{2-x}Li_xO_4$ ($x = 0, 0.05, 0.10, 0.15$) (a) and $LiMn_{1.9-y}Li_{0.1}Ni_yO_4$ ($y = 0, 0.05, 0.10, 0.15, 0.20$) (b).

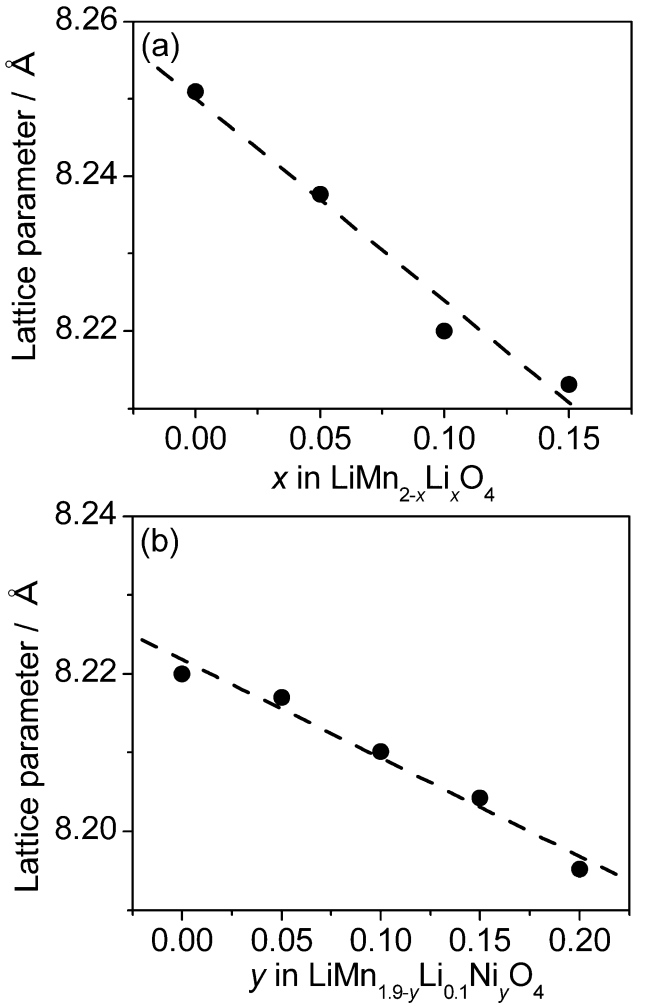

Fig. 2 Plots of cubic lattice parameter against content of low valent cation in $LiMn_{2-x}Li_xO_4$ ($x = 0, 0.05, 0.10, 0.15$) (a) and $LiMn_{1.9-y}Li_{0.1}Ni_yO_4$ ($y = 0, 0.05, 0.10, 0.15, 0.20$) (b).

valent cation content. The actually observed opposite tendency indicates that the manganese oxidation from Mn^{3+} (0.785 Å) to Mn^{4+} (0.670 Å) due to the charge compensation mainly have an effect on the lattice parameter. The XRD patterns of F^--substituted co-cation doped lithium manganese spinel oxides $LiMn_{1.8}Li_{0.1}Ni_{0.1}O_{4-\eta}F_\eta$ ($\eta = 0, 0.018, 0.036, 0.055, 0.073, 0.110, 0.180$) are shown in Fig. 3, in which the composition of the F^- ion was estimated with X-ray photoelectron spectroscopy (XPS). The spinel phase was observed in the composition range from $x = 0$ to $x = 0.073$. For $x > 0.073$, an impurity peak at around $2\theta = 30°$ was observed. It has been reported that this peak has been derived from Mn_5O_8.[18] Fig. 4 shows the variation of the lattice parameter against the F^- content. As shown in this figure, the lattice parameter was increased monotonically with increasing the F^- content until $\eta = 0.073$, although the ionic radius of F^- is smaller than that of O^{2-}. When O^{2-} was replaced by F^-, the cation charge would be compensated by the reduction of Mn^{4+} to Mn^{3+}, which leads to the increased lattice parameter for the fluorinated compounds.

3.2. Electronic structure

The Mn K-edge XANES spectra of $LiMn_{2-x}Li_xO_4$ ($x = 0, 0.05, 0.10, 0.15$) are shown in Fig. 5(a). The spectra of MnO_2 and Mn_2O_3 are also shown in Fig. 5(a) as references for Mn^{4+} and Mn^{3+}, respectively. In this figure, the main peak appeared at about 6550 eV represented the electron dipole transition from 1 s to 4p orbital.[26,27] The small intensity peak appeared at around 6540 eV could be also measured, and represented the quadrupole transitions from the core Mn 1 s orbital to the unoccupied Mn 3d orbital and/or the dipole transition to the hybridized Mn 4p-3d orbital.[26] The shape of Mn K-edge XANES spectra did not depend on the composition x, hence Mn ions is considered to exist in the octahedral 16d site.[26] The absorption-edge energies of $LiMn_{2-x}Li_xO_4$ laid between the spectra of MnO_2 and Mn_2O_3, hence the Mn ions in $LiMn_{2-x}Li_xO_4$ were the mixture of Mn^{3+} and Mn^{4+}. The absorption edge shifted toward large energy levels with the increase of the Li^+ ion content. This result indicates that the amount of Mn^{4+} increased as suggested in the XRD result shown in Fig. 2(a). Fig. 5(b) and 5(c) show the Mn and Ni K-edge spectra of $LiMn_{1.9-y}Li_{0.1}Ni_yO_4$ ($y = 0, 0.05, 0.10, 0.15, 0.20$), respectively. In the Ni K-edge spectra (Fig. 5(c)), there was no shift of absorption edge energy, hence the valence of Ni ion maintained divalent with the increase of the Li^+ ion content. On the other hand, the absorption edge of Mn K-edge XANES spectra in $LiMn_{1.9-y}Li_{0.1}Ni_yO_4$ shifted toward large energy levels with the

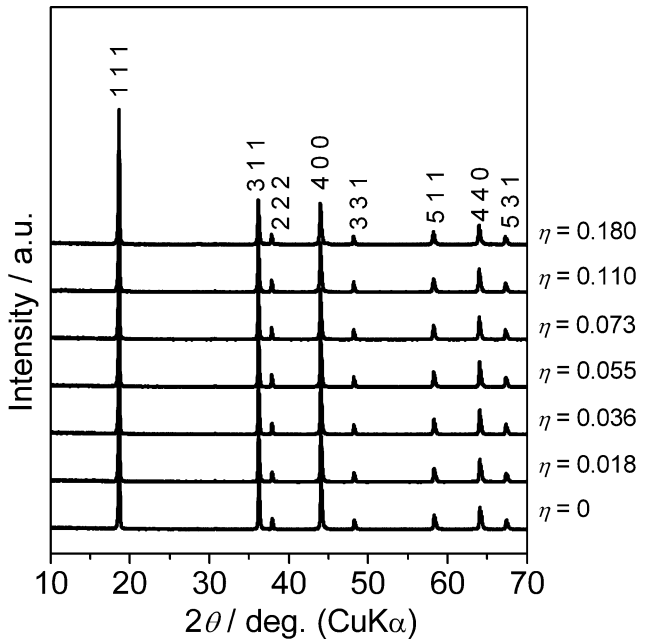

Fig. 3 Powder XRD patterns of $LiMn_{1.8}Li_{0.1}Ni_{0.1}O_{4-\eta}F_{\eta}$ (η = 0, 0.018, 0.036, 0.055, 0.073, 0.110, 0.180).

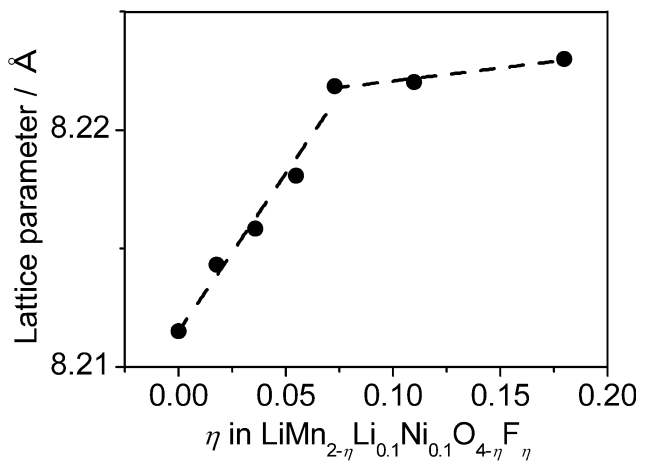

Fig. 4 Plots of lattice parameter against content of F^- in $LiMn_{1.8}Li_{0.1}Ni_{0.1}O_{4-\eta}F_{\eta}$ (η = 0, 0.018, 0.036, 0.055, 0.073, 0.110, 0.180).

increment of the Ni^{2+} ion content. Thus, the charge compensation with doping Ni ion occurred with the ratio change of Mn^{3+}/Mn^{4+} as well as $LiMn_{2-x}Li_xO_4$.

Fig. 6 shows the Mn K-edge XANES spectra of $LiMn_{1.8}Li_{0.1}Ni_{0.1}O_{4-\eta}F_{\eta}$ (η = 0, 0.036, 0.073). In the case of anion-substitution, the shape of Mn K-edge spectra did not depend on the composition η as well as $LiMn_{2-x}Li_xO_4$, as Mn ions is considered to exist in the octahedral 16d site.[26] Contrary to the effect of cation-doping, the absorption edge shifted toward smaller energy levels with the increase of the F^- content. This result indicates that the charge compensation was carried by the reduction of Mn^{4+} to Mn^{3+} and the amount of Mn^{3+} increased. Hence, it was found that the F^--substitution was effective to decrease the valence of Mn ion.

Next, the electronic structures of the cation ($Mn^{3/4+}$) and the anions (F^- and O^{2-}) were investigated by the XANES analysis.

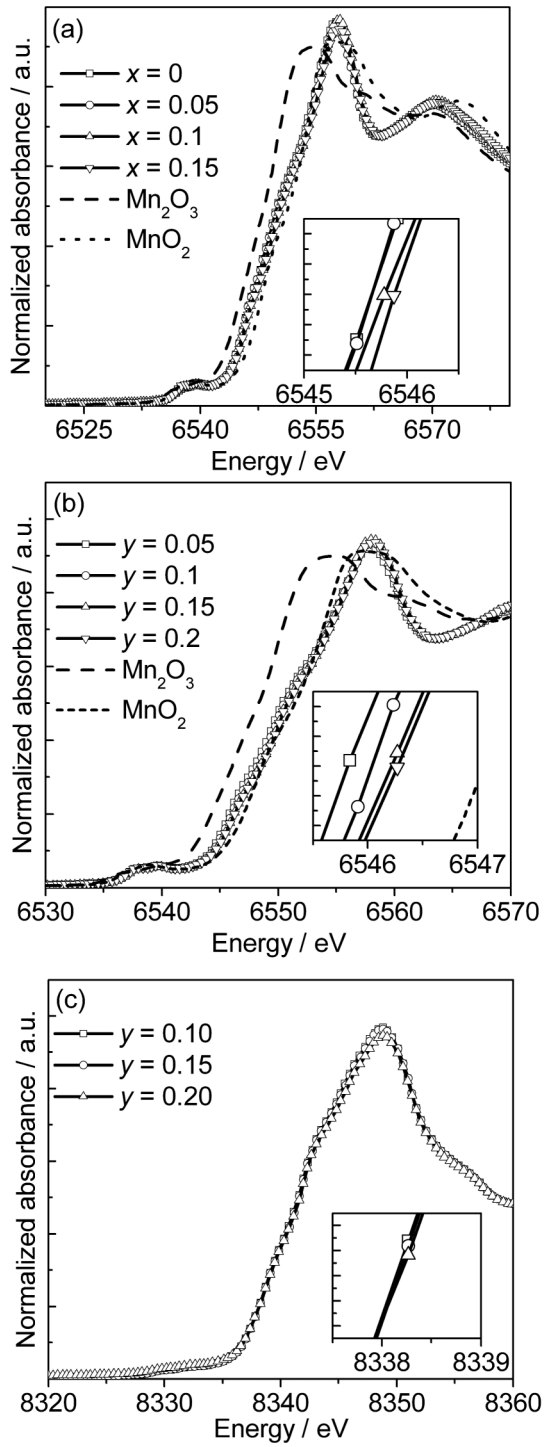

Fig. 5 XANES spectra of Mn K-edge of $LiMn_{2-x}Li_xO_4$ (x = 0, 0.05, 0.10, 0.15) (a), $LiMn_{1.9-y}Li_{0.1}Ni_yO_4$ (y = 0, 0.05, 0.10, 0.15, 0.20) (b), and Ni K-edge of $LiMn_{1.9-y}Li_{0.1}Ni_yO_4$ (y = 0, 0.05, 0.10, 0.15, 0.20) (c).

O K- and F K-edge XANES spectra were measured to consider the electronic structures in $LiMn_{1.8}Li_{0.1}Ni_{0.1}O_{4-\eta}F_{\eta}$ (η = 0, 0.036, 0.073) since it was expected that the electronic structure of the hybridized orbital between Mn and O (or F) ions revealed the anion-substitution effect and the related phenomena. Fig. 7(a) and 7(b) show the O K- and F K-edge XANES spectra of $LiMn_{1.8}Li_{0.1}Ni_{0.1}O_{4-\eta}F_{\eta}$ (η = 0, 0.036, 0.073). In the O K-edge

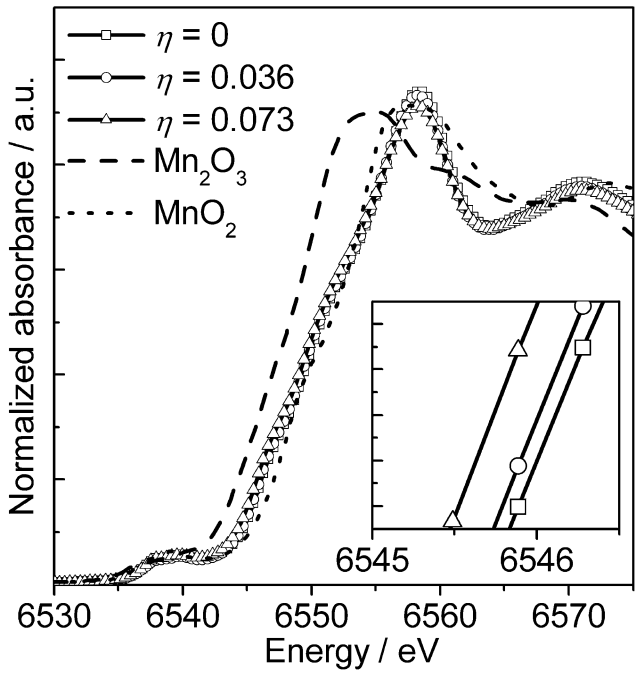

Fig. 6 XANES spectra of Mn *K*-edge of $LiMn_{1.8}Li_{0.1}Ni_{0.1}O_{4-\eta}F_{\eta}$ ($\eta = 0$, 0.036, 0.073).

spectra, four peaks (A–D) were observed, corresponding to the transitions from O 1 s core orbital to the unoccupied O 2p orbital with the dipole transition selection rules since the O 2p orbital was hybridized with the Mn 3d and 4sp orbitals. Therefore, the absorption peaks in O K-edge XANES reflect the ratio of unoccupied O 2p orbital connected with a Mn 3d and Mn 4sp orbital character.[28] The peaks A and B, which were observed around 526-534 eV, could be assigned to the transitions from O 1 s orbital to the hybridized orbital between O 2p - Mn 3d t_{2g} and O 2p - Mn 3d e_g, respectively. The broad peaks (C and D around 524–546 eV) could be attributed to the transition from O 1 s orbital to the hybridized orbital between O 2p and Mn 4sp orbitals.[28] The intensity of peak B increased with the increase of the F^- content. This phenomenon would be interpreted as the increase in the hole state at the oxygen site, that is, the decrease in d electron donation from the Mn ion to the hybridized orbital. Based on this result, it is suggested that O^{2-} was also associated with the charge compensation resulting from F^- substitution and the nature of Mn–O bonding would be influenced by F^- substitution. On the other hand, in the F K-edge spectra, there was no dependency on the F^- content in the shape and absorption edge energy. This result indicates that the electron in the fluorine orbital was strongly localized.

The XANES spectra were measured also for the delithiated $LiMn_2O_4$-type compounds since the electronic structure of hybridized orbital between Mn and O ions would reveal the phenomena during lithium-ion deintercalation. The samples of the ex-situ XAS measurement were prepared during the first charge process and the lithium content of each sample is shown in Supporting Information.

The Mn K-edge XANES spectra of $Li_{1-z}Mn_2O_4$ and $Li_{1-z}Mn_{1.8}Li_{0.1}Ni_{0.1}O_4$ at various charged states are shown in Fig. 8(a) and (b), respectively. The Mn ions occupied in the octahedral

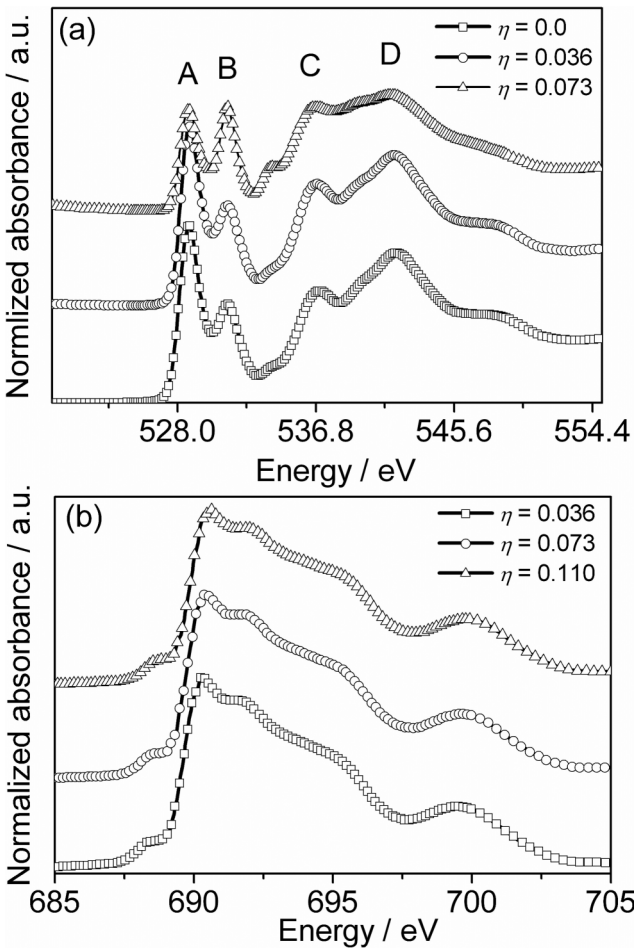

Fig. 7 XANES spectra of O K-edge (a) and F K-edge (b) of $LiMn_{1.8}Li_{0.1}Ni_{0.1}O_{4-\eta}F_{\eta}$ ($\eta = 0$, 0.036, 0.073, 0.110).

16d site were maintained during delithilated Li^+ ion since the shape of Mn K-edge spectra did not depend on the composition *z*. The absorption edge shifted toward large energy levels with decrease of the lithium ion content, which indicates that the amount of Mn^{4+} increased. This result shows that the charge variation by lithium-ion extraction/insertion was compensated by the redox of Mn^{3+}/Mn^{4+} couple.

Fig. 9 shows the Mn L- and O K-edge XANES spectra of $Li_{1-z}Mn_2O_4$ and $Li_{1-z}Mn_{1.8}Li_{0.1}Ni_{0.1}O_4$ at various discharged states. The Mn L-edge spectra for $Li_{1-z}Mn_2O_4$ and $Li_{1-z}Mn_{1.8}Li_{0.1}Ni_{0.1}O_4$ (Fig. 9(a) and (c)) consist of two sets of peaks, L_3 (A, B) and L_2 (C) separated by *ca.* 10 eV. They correspond to the electronic transitions from the $2p^{3/2}$ and $2p^{1/2}$ sites to an unoccupied 3d state. The L_2-edge peak C was more broadened than those of the L_3-edge (A, B). This difference has been explained by Coster-Kronig Auger decay.[29] A shorter lifetime of the $2p^{1/2}$ core hole due to a radiationless electron transition from the $2p^{2/3}$ to the $2p^{1/2}$ level, accompanies by the promotion of a valence electron into the conduction band. There were two peaks in the L_3-edge since the Mn 3d orbital splits to t_{2g} (A) and e_g (B) states by the ligand field theory under octahedral (O_h) symmetry.[29] The absorption edge shifted toward lower energy levels with the increase of *z* value, that is, the decrement of the lithium-ion content, indicating that number of Mn^{4+} was increased by reduction of Mn^{3+}. Focusing

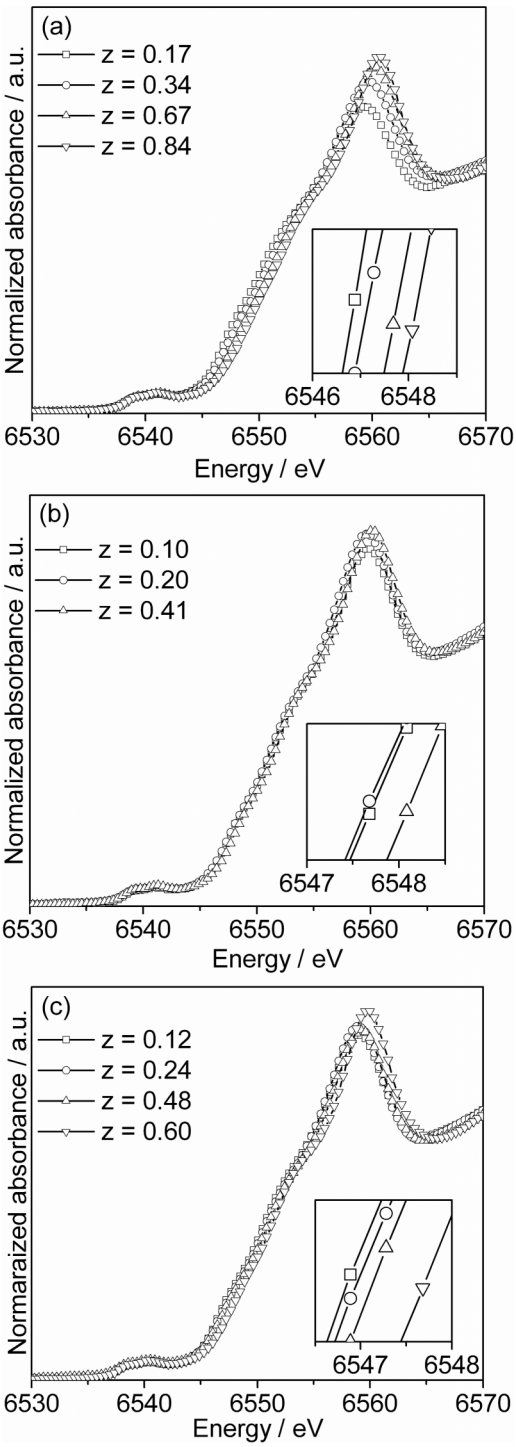

Fig. 8 Ex-situ XANES spectra of Mn K-edge for $Li_{1-z}Mn_2O_4$ (a) $Li_{1-z}Mn_{1.8}Li_{0.1}Ni_{0.1}O_4$ (b) and $Li_{1-z}Mn_{1.8}Li_{0.1}Ni_{0.1}O_{3.964}F_{0.036}$ (c) at various discharge state.

on the L_3-edge, the increase of peak A upon electrochemical lithium-ion extraction indicates that the electron is ejected from the occupied Mn 3d t_{2g} orbital, that is, the oxidation state of Mn ion increases. These results represent that the charge variation by the lithium-ion extraction was compensated by the redox of the Mn^{3+}/Mn^{4+} couple and the degree of hybridization between Mn and oxide ions in $Li_{1-z}Mn_2O_4$ and $Li_{1-z}Mn_{1.8}Li_{0.1}Ni_{0.1}O_4$ was influenced by the lithium-ion extraction process.

In the case of O K-edge spectra, four main peaks (A–D) were observed. Peaks A and B corresponded to the Mn 3d/O 2p hybridized orbital and peaks C and D were ascribed to the Mn 4sp/O 2p hybridized orbital, as described above. The intensity of peak A seems to increase with decrease of the Li^+ ion content. This phenomenon would be interpreted that the electron is released from the Mn 3d/O 2p hybridized orbital, as the Li^+ ion is extracted from the spinel manganese. A few peaks are observed in addition to the main four peaks in the O K-edge spectra of the delithiated samples. This would come from the reformation of the hybridized orbital between Mn and O ions. All the peaks dramatically change with the extraction of Li^+ ion. Hence, it is considered that O^{2-} is also associated with the charge compensation during charge and discharge process. From the result of Mn L- and O K-edge XANES spectra, it was implied that electronic charge transfer processes occur at oxide ion sites as well as Mn ion sites in $Li_{1-z}Mn_2O_4$ and $Li_{1-z}Mn_{1.8}Li_{0.1}Ni_{0.1}O_4$ upon electrochemical lithium-ion extraction. These combined results strongly suggest that these compounds are classified as the charge transfer type, which has been described for compounds containing late-transition metal ions.[30–32]

Fig. 10 shows the Mn L-, O K- and F K-edge XANES spectra of $Li_{1-z}Mn_{1.8}Li_{0.1}Ni_{0.1}O_{3.864}F_{0.036}$ at various discharged states. The Mn L- and O K- edge spectra shown in Fig. 10(a) and (b) are essentially the same as those of the fluoride-free compounds shown in Fig. 9(a) and (b). It is accordingly expected that the peak assignment should be the same. The absorption edge shifted toward higher energy levels with the decrement of the lithium-ion content. This result indicates that number of Mn^{4+} is increased by the reduction of Mn^{3+}, which could also observed at Mn K-edge XANES spectra (Fig. 8(c)). The increased intensity of peak B in Fig. 10(b) with delithiation suggests that the hole state at the oxygen site is increased with delithiation and thus the oxide ions contribute to the charge compensation during charge and discharge process. On the other hand, there is no dependency in the shape and absorption edge energy in the F K-edge spectra on delithiation. Note that, the XANES spectrum shapes of delithiated samples in Fig. 10(c) looks different from those of pristine ones in Fig. 7(b). It would be comes from the difference of background between both samples since the areas radiated active materials in delithiated samples were less as well as the amount of fluoride ion is small in the samples. This result indicates that the strongly localized fluorine orbital would not change during delithiation. From these results, it is implied that electronic transfer processes occur at oxide ion sites as well as Mn ion sites in $Li_{1-z}Mn_{1.8}Li_{0.1}Ni_{0.1}O_{3.954}F_{0.036}$ as well as $Li_{1-z}Mn_2O_4$ and $Li_{1-z}Mn_{1.8}Li_{0.1}Ni_{0.1}O_4$ upon electrochemical lithium-ion insertions. However, F 2p orbital is localized and do not effect on the electron exchange with lithium insertion/deinsertion.

3.3. Local structure

In order to investigate the local structures around Mn atom and Ni atom in $LiMn_{2-x}Li_xO_4$, $LiMn_{1.9-y}Li_{0.1}Ni_yO_4$ and $LiMn_{1.8}Li_{0.1}Ni_{0.1}O_{4-\eta}F_\eta$, Mn and Ni K-edge EXAFS spectra were measured.

Fig. 11 (a) and (b) shows Fourier transforms (FTs) of the EXAFS oscillations in $LiMn_{2-x}Li_xO_4$ ($x = 0$, 0.05, 0.10, 0.15) and $LiMn_{1.9-y}Li_{0.1}Ni_yO_4$ ($y = 0$, 0.05, 0.10, 0.15, 0.20) which represent

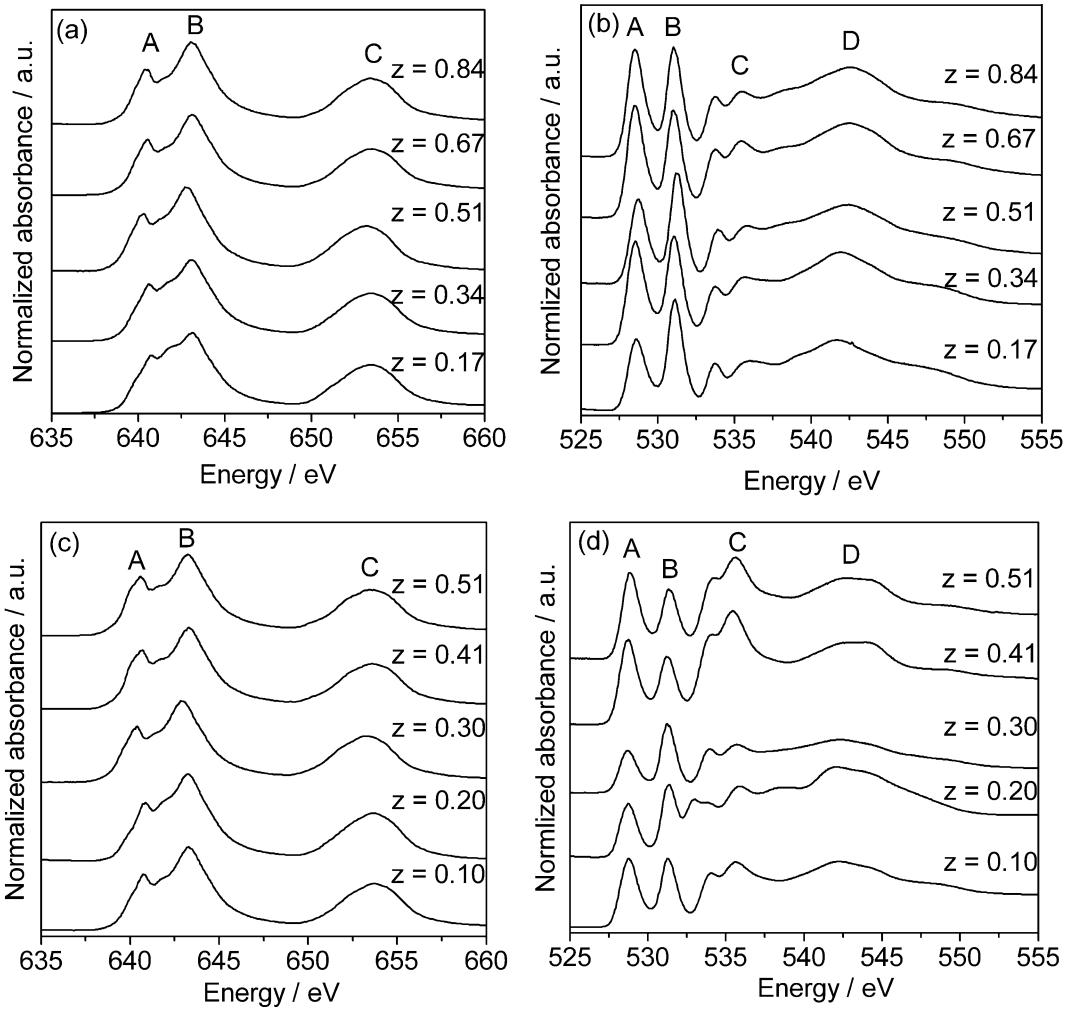

Fig. 9 Ex-situ XANES spectra of Mn L-edge (a) and O K-edge (b) for $Li_{1-z}Mn_2O_4$, and Mn K-edge (c) and O K-edge (d) for $Li_{1-z}Mn_{1.8}Li_{0.1}Ni_{0.1}O_4$ at various discharge state.

the pseudo-radial structure functions (RSFs) of the local atomic environments around the Mn atoms. The FTs of the k^3-weighted Mn K-edge EXAFS oscillations for samples were calculated within k = 3.5–14.0 Å^{-1} (this range was chosen to minimize noise). The RSFs of Mn K-edge EXAFS show two peaks at about 1.6 and 2.6 Å, respectively. The first and second peaks for the Mn K-edge spectra correspond to six coordinated Mn–O bonds in the MnO_6 octahedron and Mn–M (Metal) interactions, respectively. As for the Mn–O peak, the intensity was increased with increasing the cation content in both spectra. The intensity of Mn–M peak for $LiMn_{2-x}Li_xO_4$ did not show clear tendency while that for $LiMn_{1.9-y}Li_{0.1}Ni_yO_4$ was enhanced with increasing the Ni content.

The RSFs around the Mn atoms were inversely Fourier-filtered over the two peaks (R = 1.1–3.0 Å) in the transformation and fitted with equation (1). The structural parameters were determined using curve-fitting, and the atomic distances and DW factors in $LiMn_{2-x}Li_xO_4$ were compared with the x values as shown in Fig. 12. The bond length was decreased with the increase of Li^+ ion content. This is due to the oxidation of Mn from Mn^{3+} to Mn^{4+}, which has already been indicated by the peak shift of Mn L-edge XANES. Shannon's ionic radius of Mn^{3+} and Mn^{4+} is 0.65 Å and 0.53 Å, respectively.[25] In addition, the inter-atomic lengths of Mn–M decreased with the lithium-ion extraction. Hence, MnO_6 octahedral would shrink with the increment of the Li^+ ion content. This is also consistent with the XRD results. The DW factors for the Mn–O interaction decreased with the decrement of the lithium-ion content of the samples, indicating that the distortion of MnO_6 octahedra decreased. The Jahn–Teller distortion of Mn^{3+} effects on this phenomenon. The DW factor for the Mn–M interaction was invariant with x. This phenomenon will be reconsidered below.

The same procedure was applied to $LiMn_{1.9-y}Li_{0.1}Ni_yO_4$ and the atomic distances and DW factors in $LiMn_{1.9-y}Li_{0.1}Ni_yO_4$ were compared with the y values as shown in Fig. 13. The Mn–O and Mn–M lengths were decreased with the increase of Ni^{2+} ion contents. This is due to the oxidation of Mn from Mn^{3+} to Mn^{4+}.

The DW factor for each interaction (Mn–O, Mn–Mn) decreased with the Ni substitution, indicating the decrement of the MnO_6 octahedra distortion. For the local structure around Ni, there are no remarkable changes in the Ni K-edge spectra with the Ni content as shown in Fig.11(c). As shown in Fig. 13, the Ni–O and Ni-M distance, as well as the DW factors, did not change with the Ni content. This reason would be that the doped Ni ion remained divalent at any Ni content. Based on these results, it is revealed that the local distortion around Mn was decreased by cation doping,

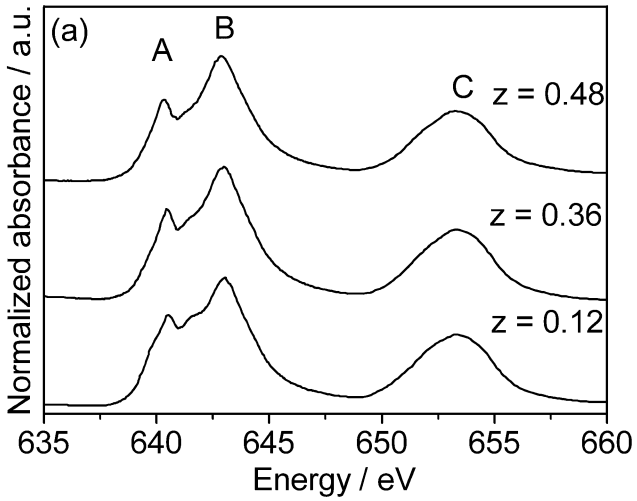

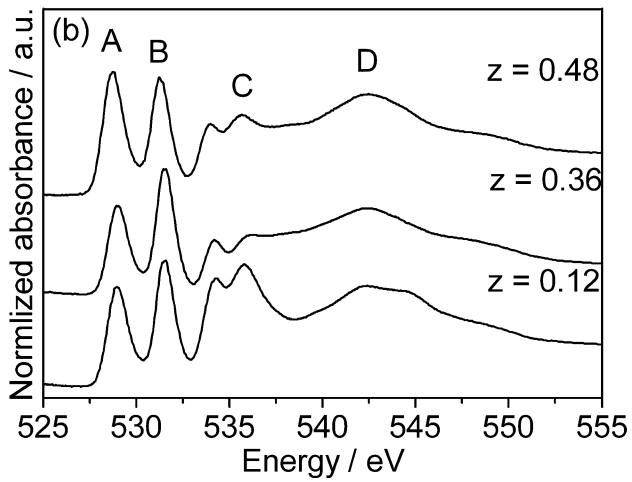

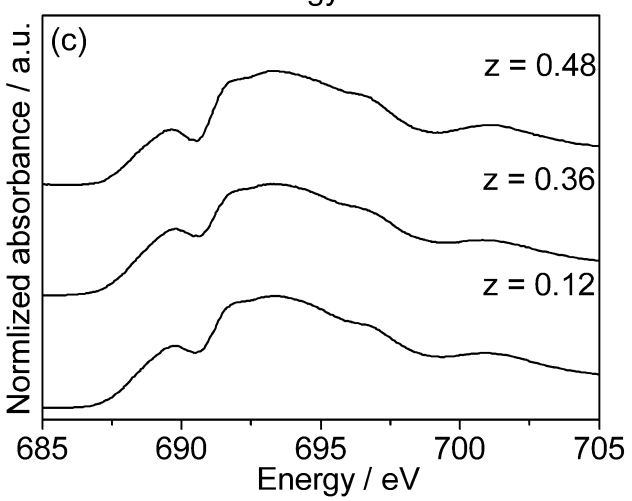

Fig. 10 Ex-situ XANES spectra of Mn L-edge (a), O K-edge (b) and F K-edge for $Li_{1-z}Mn_{1.8}Li_{0.1}Ni_{0.1}O_{3.964}F_{0.036}$ at various discharge state.

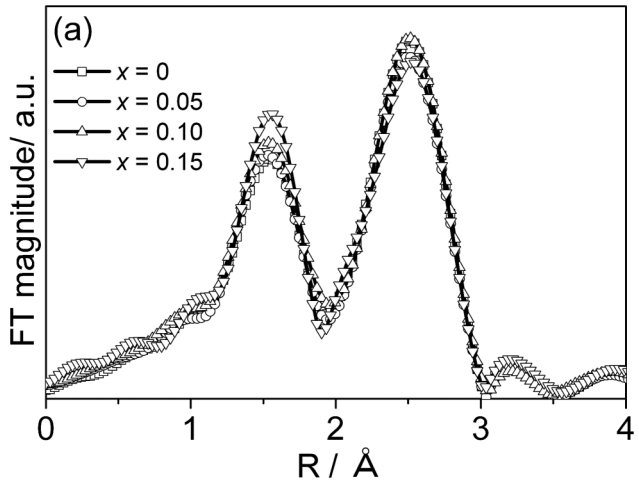

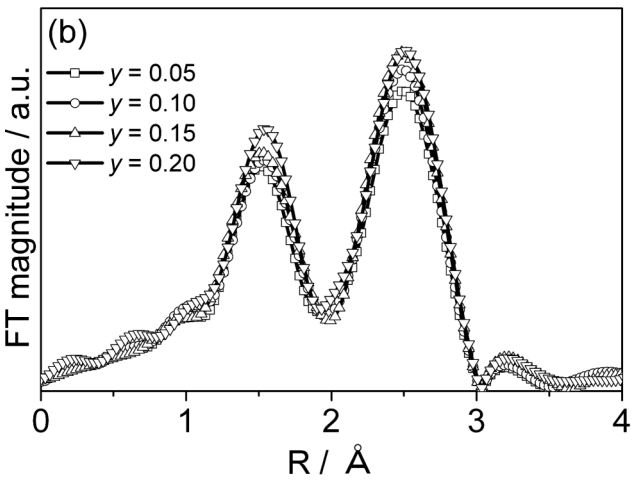

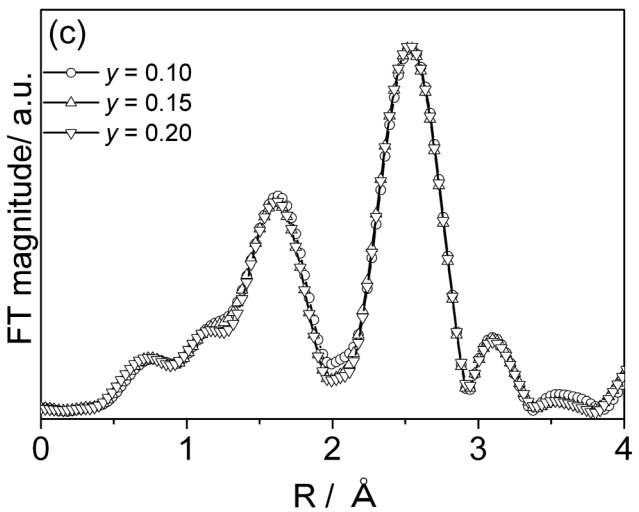

Fig. 11 EXAFS spectra of Mn K-edge of $LiMn_{2-x}Li_xO_4$ ($x = 0, 0.05, 0.10, 0.15$) (a) and $LiMn_{1.9-y}Li_{0.1}Ni_yO_4$ ($y = 0, 0.05, 0.10, 0.15, 0.20$) (b), and Ni K-edge of $LiMn_{1.9-y}Li_{0.1}Ni_yO_4$ ($y = 0, 0.05, 0.10, 0.15, 0.20$) (c).

since the number of Mn^{3+}, which is the Jahn–Teller cation, was decreased. The DW factor of Mn–M for $LiMn_{2-x}Li_xO_4$ remained constant, but that for $LiMn_{1.9-y}Li_{0.1}Ni_yO_4$ was decreased with the increase of cation content. This difference is probably due to the fact that Li^+ is larger than that of Ni^{2+}; hence the influence of doped Li^+ would not be observed at 2nd neighborhood for local distortion. Then, the influence of F^--doping on the local structure was investigated. Fig. 14 shows the FT of EXAFS oscillations of the Mn K-edge spectra of $LiMn_{1.8}Li_{0.1}Ni_{0.1}O_{4-\eta}F_\eta$ ($\eta = 0.0, 0.036, 0.073$). The intensities of Mn–O(F) and Mn–M peaks were decreased with increasing of the F^- content. Fig. 15 shows the variation of interatomic distances and DW factors against the F^- content. The Mn–O(F) and Mn–M distances were monotonically

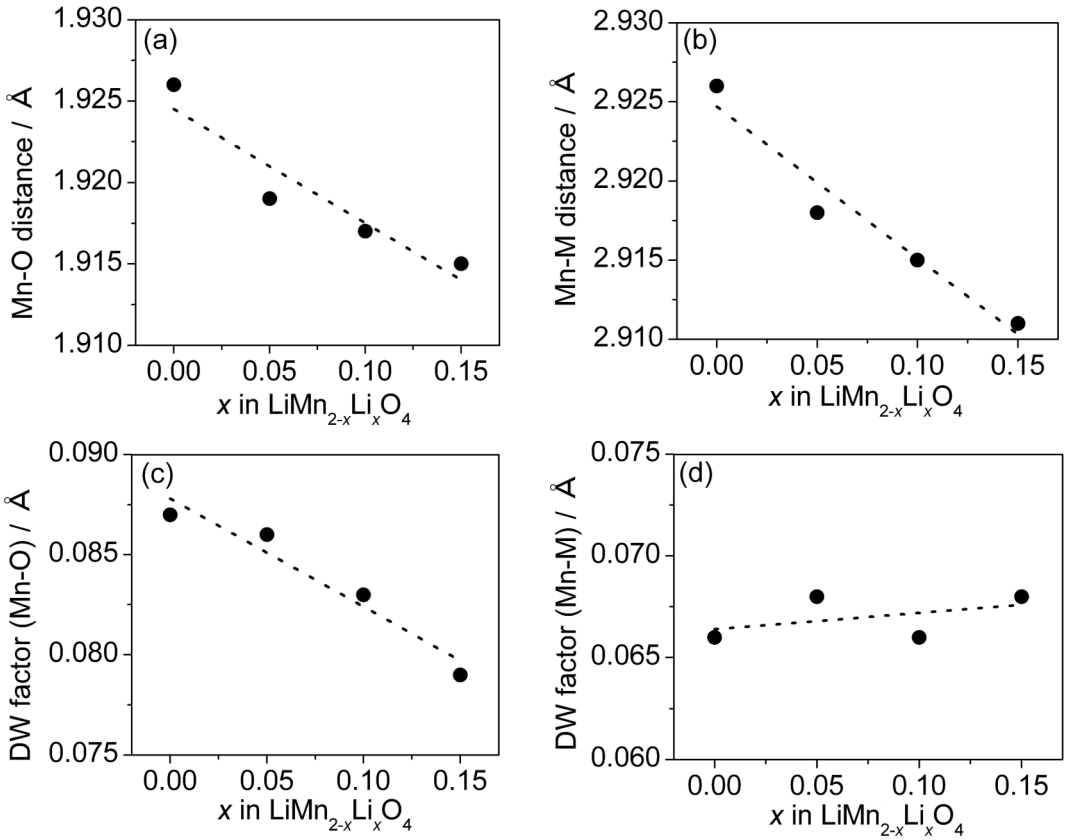

Fig. 12 Plots of inter-atomic distances ((a) Mn–O and (c) Mn–M) and Debye–Waller (DW) factors ((b) Mn–O and (d) Mn–M) of $LiMn_{2-x}Li_xO_4$ ($x = 0$, 0.05, 0.10, 0.15) obtained by EXAFS analysis of Mn K-edge spectra.

increased with the increase of the F^- content due to the decrease of Mn^{4+} ion. The DW factors of both Mn–O(F) and Mn–M were increased, which indicated that local distortion around the Mn ion was increased. This is due to the increase of Mn^{3+} (Jahn–Teller) formed by the charge compensation. Based on the XAFS measurement, it was clarified that the effect of F^- substitution on the electronic/local structure was opposite to the low valence cation-doping.

The FTs of EXAFS oscillations of the Mn K-edge spectra of the delithiated $Li_{1-z}Mn_2O_4$, $Li_{1-z}Mn_{1.8}Li_{0.1}Ni_{0.1}O_4$ and $Li_{1-z}Mn_{1.8}Li_{0.1}Ni_{0.1}O_{3.964}F_{0.036}$ samples at various discharged states are shown in Fig. 16. The first and second peaks correspond to Mn–O and Mn–M bonds (M = Mn, Li, and Ni), respectively. As for the Mn–O peak, the intensity was increased with decreasing of the Li^+ ion content in these spectra. Fig. 17 shows the variation of interatomic distances and DW factors against the Li^+ ion content. The Mn–O and Mn–M distance were monotonically decreased with decrease of the Li content due to the increase of Mn^{4+}. This result is corresponding to the decreased lattice parameters obtained from the XRD measurement. The DW factors of Mn–O were decreased monotonically with the decrease of Li^+ ion contents. Based on the result, it was revealed that the local distortion around Mn ion was decreased by the extraction of Li^+ ion, since the number of Mn^{3+}, which is Jahn–Teller cation, was decreased.

Next, we compare the degree of the DW factors for $Li_{1-z}Mn_2O_4$, $Li_{1-z}Mn_{1.8}Li_{0.1}Ni_{0.1}O_4$ and $Li_{1-z}Mn_{1.8}Li_{0.1}Ni_{0.1}O_{3.964}F_{0.036}$. The degree of the DW factor in $Li_{1-z}Mn_{1.8}Li_{0.1}Ni_{0.1}O_4$ was smaller than that in $Li_{1-z}Mn_2O_4$. This is because of the smaller amount of the Jahn–Teller cation (Mn^{3+} ion) in the pristine $LiMn_{1.8}Li_{0.1}Ni_{0.1}O_4$ than $LiMn_2O_4$. On the other hand, the degree of the DW factor in $Li_{1-z}Mn_{1.8}Li_{0.1}Ni_{0.1}O_{3.964}F_{0.036}$ was similar to that in $Li_{1-z}Mn_{1.8}Li_{0.1}Ni_{0.1}O_4$, although the amount of the Mn^{3+} ion in $LiMn_{1.8}Li_{0.1}Ni_{0.1}O_{3.964}F_{0.036}$ was greater than that in $LiMn_{1.8}Li_{0.1}Ni_{0.1}O_4$. It is considered that the F^- ion doping prevents the local distortion around Mn atom during the redox reaction (Mn^{3+}/Mn^{4+}) in $LiMn_{1.8}Li_{0.1}Ni_{0.1}O_{3.964}F_{0.036}$.

Based on the ex-situ XAFS measurements, it was clarified that the structural relaxation with F^- ion doping is crucial to the local structural change during Li^+ ion extraction as well as the amount of Jahn–Teller Mn^{3+} cations.

3.4. Electrochemical Properties

Fig. 18 shows the 1st charge and discharge curves of $LiMn_2O_4$, $LiMn_{1.8}Li_{0.1}Ni_{0.1}O_4$, and $LiMn_{1.8}Li_{0.1}Ni_{0.1}O_{4-\eta}F_\eta$ (η = 0.036, 0.073). The order of the capacity was $LiMn_2O_4$ > $LiMn_{1.8}Li_{0.1}Ni_{0.1}O_{4-\eta}F_\eta$ ($\eta = 0.073$) > $LiMn_{1.8}Li_{0.1}Ni_{0.1}O_{4-\eta}F_\eta$ (η = 0.036) > $LiMn_{1.8}Li_{0.1}Ni_{0.1}O_4$, which has been also reported before.[33] This order is corresponding to the number of Mn^{3+} in the pristine material obtained by the XANES results. Hence, it is confirmed that the increment of Mn^{3+} ion by the substitution of F^- ion is effective to increase the discharge capacity.

Fig. 19 shows the cycle performance of $LiMn_2O_4$, $LiMn_{1.8}Li_{0.1}Ni_{0.1}O_4$, and $LiMn_{1.8}Li_{0.1}Ni_{0.1}O_{4-\eta}F_\eta$ (η = 0.036). Although $LiMn_2O_4$ showed a large capacity at early cycles, the

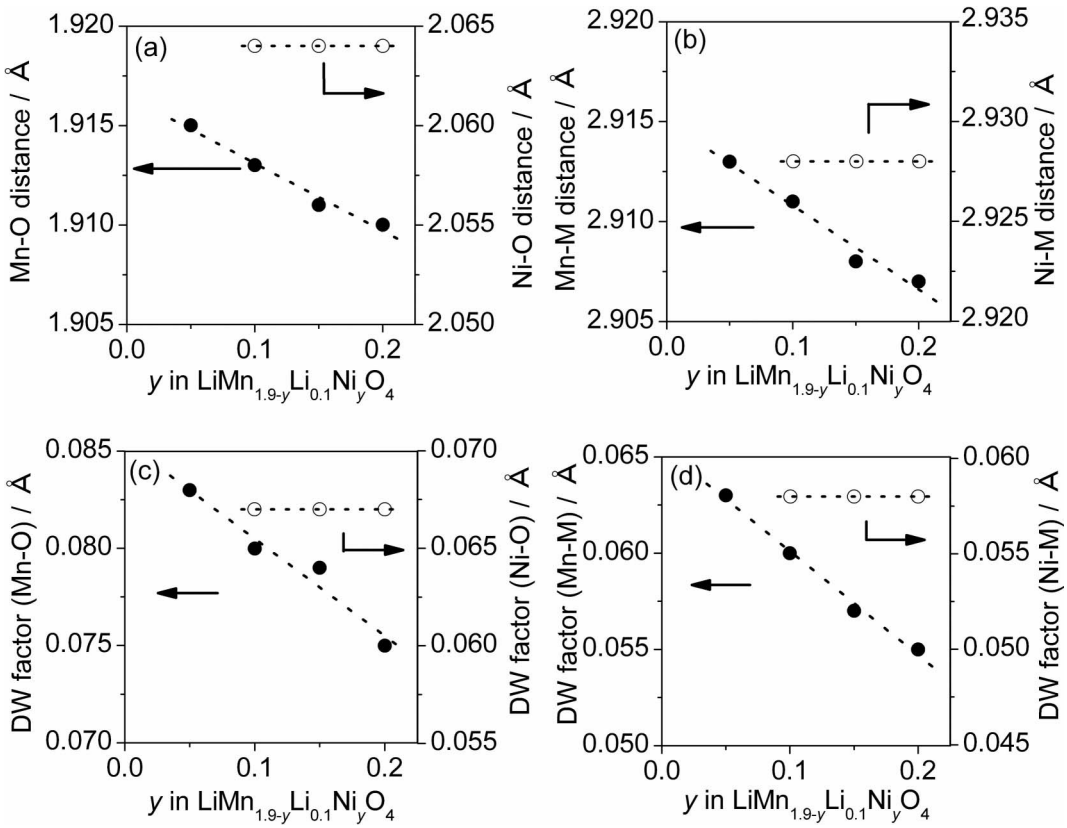

Fig. 13 Plots of inter-atomic distances ((a) Mn–O (closed cycle) and Ni–O (open cycle), (c) Mn-*M* (closed cycle) and Ni-*M*) and Debye–Waller (DW) factors ((b) Mn–O (closed cycle) and Ni–O (open cycle), (d) Mn-*M* (closed cycle) and Ni-*M* (open cycle)) of $LiMn_{1.9-y}Li_{0.1}Ni_yO_4$ (y = 0, 0.05, 0.1, 0.15, 0.2) obtained by EXAFS analysis of Mn and Ni K-edge spectra.

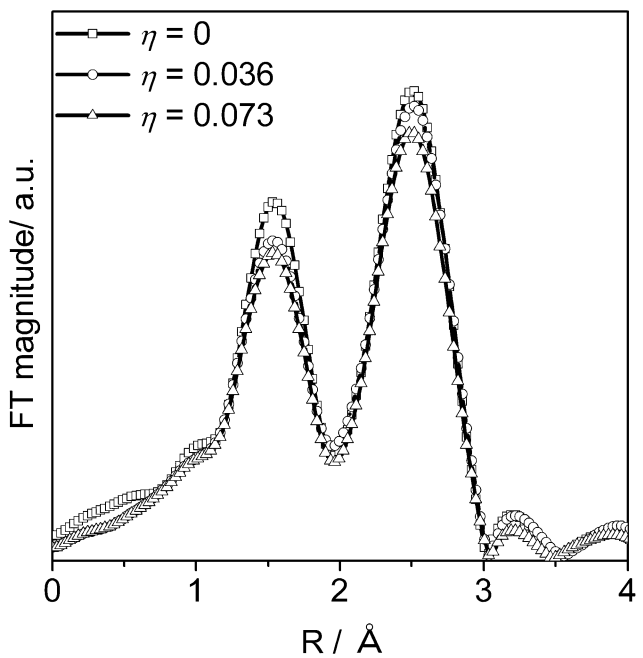

Fig. 14 EXAFS spectra of Mn K-edge of $LiMn_{1.8}Li_{0.1}Ni_{0.1}O_{4-\eta}F_\eta$ (η = 0, 0.036, 0.073).

capacity decreased rapidly. On the contrary, $LiMn_{1.8}Li_{0.1}Ni_{0.1}O_4$ showed a small capacity but good cycleability. This result is explained as follows. For $LiMn_2O_4$, a large distortion of the MnO_6 octahedrons, which were shown as the Debye–Waller factors in Fig. 17, is responsible for the insufficient cycle performance. Low valence cation-doping in $LiMn_{1.8}Li_{0.1}Ni_{0.1}O_4$ imparts the cycleability by the decrease of the local distortion of Jahn–Teller Mn^{3+} ion.

A relatively high capacity were fortunately obtained in $LiMn_{1.8}Li_{0.1}Ni_{0.1}O_{4-\eta}F_\eta$ (η = 0.036). The large capacity results from the increment of the Mn^{3+} ion. Moreover, a relatively good cycleability was also observed, while the increment of Jahn–Teller Mn^{3+} ion is deemed as the problem for cycleability. The F^- ion doping could prevent the MnO_6 octahedra distortion and thus serve the improvement in cycleability.

In order to improve the electrochemical performance of the spinel lithium manganese oxides, anion substitution would be one of the effective methods when combined with low valence cation-doping.

Conclusions

In order to clarify the effect of anion-substitution for spinel lithium manganese oxides on the electrochemical performance, the electronic and local structures of $LiMn_{2-x}Li_xO_4$, $LiMn_{1.9-y}Li_{0.1}Ni_yO_4$ and $LiMn_{1.8}Li_{0.1}Ni_{0.1}O_{4-\eta}F_\eta$ were investigated using X-ray absorption spectroscopy. The atomic distance between Mn and O was decreased with the increase of doped low valence cation (Li or Ni) content. This is due to the increase of Mn^{4+} formed by charge

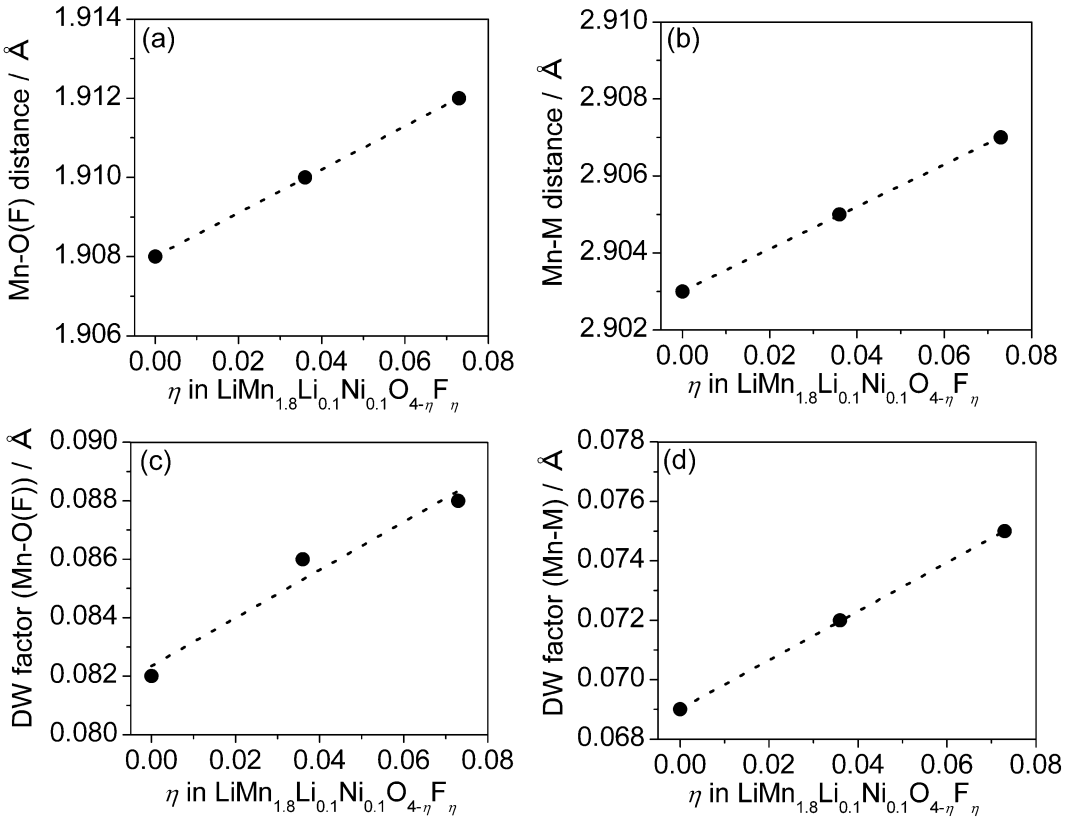

Fig. 15 Plots of atomic distances ((a) Mn–O(F) and (c) Mn–M) and Debye–Waller (DW) factor ((b) Mn–O(F) and (d) Mn–M) of $LiMn_{1.8}Li_{0.1}Ni_{0.1}O_{4-\eta}F_{\eta}$ ($\eta = 0$, 0.036, 0.073) obtained by EXAFS analysis of Mn K-edge spectra.

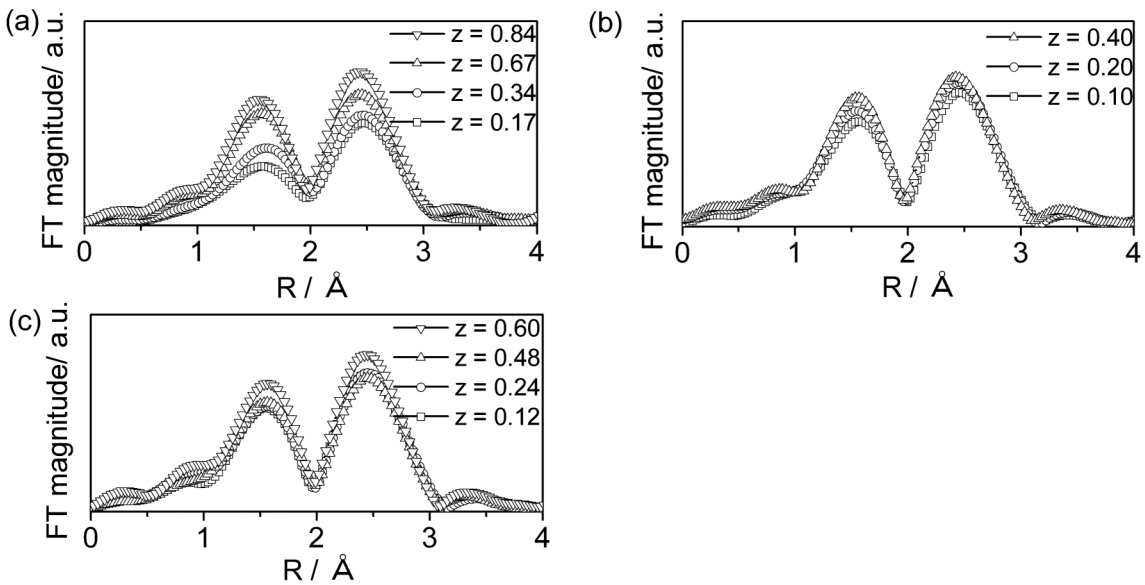

Fig. 16 Ex-situ EXAFS spectra of Mn K-edge for $Li_{1-z}Mn_2O_4$ (a), $Li_{1-z}Mn_{1.8}Li_{0.1}Ni_{0.1}O_4$ (b) and $Li_{1-z}Mn_{1.8}Li_{0.1}Ni_{0.1}O_{3.964}F_{0.036}$ (c) at various discharge state.

compensation (oxidation of Mn^{3+} to Mn^{4+}). The local distortion around Mn ion was decreased, since the number of Mn^{3+}, which is a Jahn–Teller ion, was decreased. On the contrary, the distance between Mn and O(F) was increased with increase of F^- content. This is due to the increase of Mn^{3+} formed by charge compensation (reduction of Mn^{4+} to Mn^{3+}).

The charge and discharge performance is strongly related with electronic structure around Mn ion, and F^- ion substitution makes the capacity increment. Furthermore, the degradation of cycleability with the effect of Jahn–Teller Mn^{3+} ion could be prevented by the F^- ion substitution. Therefore, designation of suitable anion substitution and low valence cation-doping

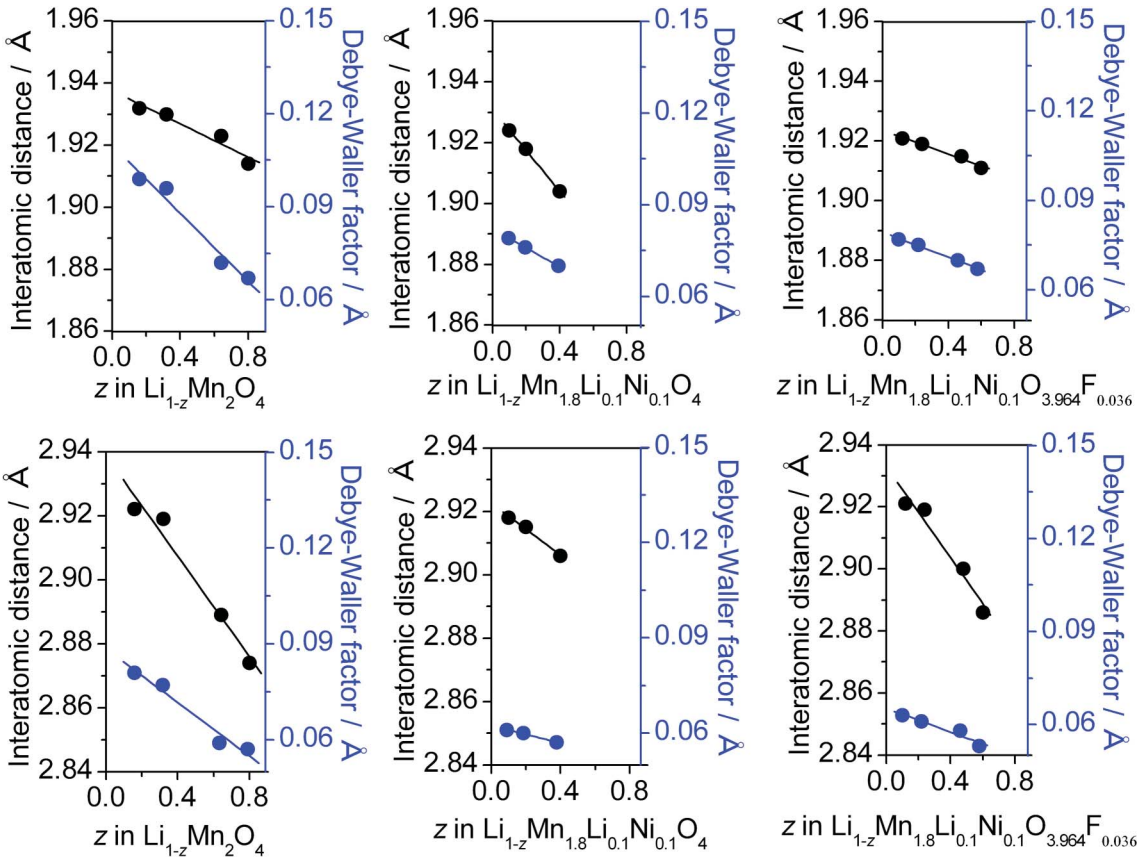

Fig. 17 Plots of inter-atomic distances and Debye–Waller (DW) factors of (Mn–O, F and Mn–M) of $Li_{1-z}Mn_2O_4$ (a, d), $Li_{1-z}Mn_{1.8}Li_{0.1}Ni_{0.1}O_4$ (b, e) and $Li_{1-z}Mn_{1.8}Li_{0.1}Ni_{0.1}O_{3.964}F_{0.036}$ (c, f) at various discharge states.

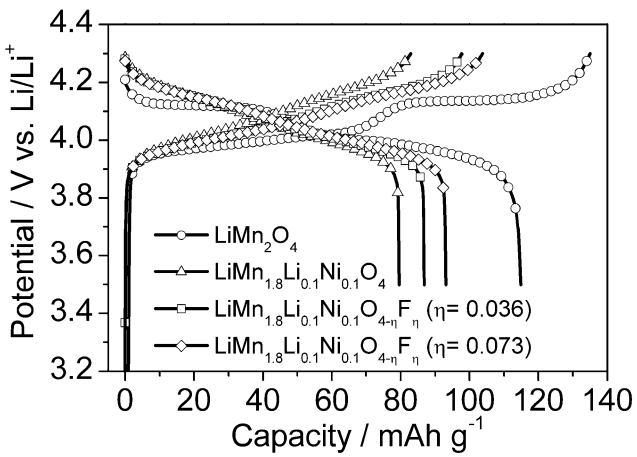

Fig. 18 Charge and discharge profile at 1st cycle of $LiMn_2O_4$, $LiMn_{1.8}Li_{0.1}Ni_{0.1}O_4$, and $LiMn_{1.8}Li_{0.1}Ni_{0.1}O_{4-\eta}F_\eta$ ($\eta = 0.036, 0.073$).

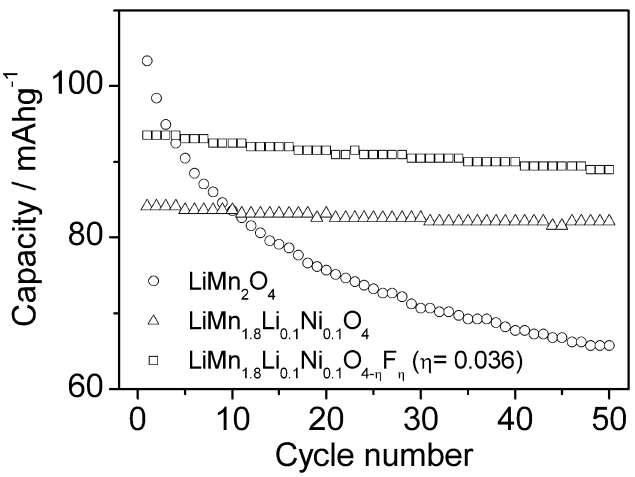

Fig. 19 Cycleability of $LiMn_2O_4$, $LiMn_{1.8}Li_{0.1}Ni_{0.1}O_4$, and $LiMn_{1.8}Li_{0.1}Ni_{0.1}O_{4-\eta}F_\eta$ ($\eta = 0.036$).

should be effective for realizing higher electrochemical performance.

Acknowledgements

Part of this work was supported by Research and Development Initiative for Scientific Innovation of New Generation Batteries (RISING) project from New Energy and Industrial Technology Department Organization (NEDO) in Japan. The authors greatly acknowledge it.

References

1 B. L. Ellis, K. T. Lee and L. F. Nazar, *Chem. Mater.*, 2010, **22**, 691.
2 T. Fukutsuka, K. Sakamoto, Y. Matsuo, Y. Sugie, T. Abe, Z. Ogumi and Electrochem, *Electrochem. Solid-State Lett.*, 2004, **7**, A481.

3 J. Gummow, A. deKock and M. M. Thackeray, *Solid State Ionics*, 1994, **69**, 59.
4 Y. Xia, Y. Zhou and M. Yoshio, *J. Electrochem. Soc.*, 1997, **144**, 2593.
5 L. Guohua, H. Ikuta, T. Uchida and M. Wakihara, *J. Electrochem. Soc.*, 1996, **143**, 178.
6 F. L. Cras, D. Bloch, M. Anne and P. Strobel, *Solid State Ionics*, 1996, **89**, 203.
7 R. J. Gummow, A. de. Kock and M. M. Thackeray, *Solid State Ionics*, 1994, **69**, 59.
8 A. D. Robertson, S. H. Lu, W. F. Averill and W. F. Jr. Howard, *J. Electrochem. Soc.*, 1997, **144**, 3500.
9 M. Kaneko, S. Matsuno, T. Miki, M. Nakayama, H. Ikuta, Y. Uchimoto, M. Wakihara and K. Kawamura, *J. Phys. Chem. B*, 2003, **107**, 1727.
10 L. Xiao, Y. Zhao, Y. Yang, Y. Cao, X. Ai and H. Yang, *Electrochim. Acta*, 2008, **54**, 545.
11 Z. Zhang, T. Yabu and I. Taniguchi, *Mater. Res. Bull.*, 2009, **44**, 707.
12 M. V. Reddy, S. S. Manoharan, J. John, B. Singh, G. V. Subba Rao and B. V. R. Chowdari, *J. Electrochem. Soc.*, 2009, **156**, A652.
13 A. Sakunthala, M. V. Reddy, S. Selvasekarapandian, B. V. R. Chowdari and P. C. Selvin, *Electrochim. Acta*, 2010, **55**, 4441.
14 K. Kubo, M. Fujiwara, S. Yamada, S. Arai and M. Kanda, *J. Power Sources*, 1997, **68**, 553.
15 S. Yonezawa, T. Okayama, H. Tsuda and M. Takashima, *J. Fluorine Chem.*, 1998, **87**, 141.
16 S. Yonezawa, M. Yamasaki and M. Takashima, *J. Fluorine Chem.*, 2004, **125**, 1657.
17 G. G. Amatucci, N. Pereira, T. Zheng, I. Plitz and J. M. Tarascon, *J. Power Sources*, 2001, **81**, 39.
18 G. G. Amatucci, A. D. Pasquier, A. Blyr, T. Zheng and J. M. Tarascon, *Electrochim. Acta*, 1999, **45**, 255.
19 W. Choi and A. Manthiram, *Electrochem. Solid-State Lett.*, 2006, **9**, A245.
20 W. Choi and A. Manthiram, *J. Electrochem. Soc.*, 2007, **154**, A792.
21 H. Oyanagi, T. Matsushida, M. Ito and H. Kuroda, *KEK Rep.*, 1984, **83**, 30.
22 Y. Kitajima, K. Amemiya, Y. Yonamoto,T. Ohta, T. Kikuchi, T. Kosuge, A. Toyoshima and K. Ito, *J. Synchrotron Radiat.*, 1998, **5**, 729.
23 T. Taguchi, T. Ozawa and H. Yashiro, *Phys. Scr.*, 2005, **T115**, 205.
24 J. J. Rehr and R. C. Albers, *Rev. Mod. Phys.*, 2000, **72**, 621.
25 R. D. Shannon, *Acta Crystallogr., Sect. A: Cryst. Phys., Diffr., Theor. Gen. Crystallogr.*, 1976, **32**, 751.
26 H. S. Park, S. J. Hwang and J. H. Choy, *J. Phys. Chem. B*, 2001, **105**, 4860.
27 N. Sung, Y. Sun, S. Kim and M. Jang, *J. Electrochem. Soc.*, 2008, **155**, A845.
28 M. Nakayama, S. Goto, Y. Uchimoto, M. Wakihara, Y. Kitajima, T. Miyanaga and I. Watanabe, *J. Phys. Chem. B*, 2005, **109**, 11197.
29 F. M. F. de Groot, J. C. Fuggle, B. T. Thole and G. A. Sawatzky, *Phys. Rev. B: Condens. Matter*, 1990, **41**, 928.
30 J. Zaanen, G. A. Sawatzky and J. W. Allen, *Phys. Rev. Lett.*, 1985, **62**, 418.
31 P. Kuiper, G. Kruizinga, J. Ghijsen, G. A. Sawatzky and H. Verweji, *Phys. Rev. Lett.*, 1989, **62**, 221.
32 J. van Elp, H. Eskes, P. Kuiper and G. A. Sawatzky, *Phys. Rev. B: Condens. Matter*, 1992, **45**, 1612.
33 K. Matsumoto, T. Fukutsuka, T. Okumura, Y. Uchimoto, K. Amezawa, M. Inaba and A. Tasaka, *J. Power Sources*, 2009, **189**, 599.

